

Haldane phase, field-induced magnetic ordering and Tomonaga-Luttinger liquid behavior in a spin-one chain compound $\text{NiC}_2\text{O}_4 \cdot 2\text{NH}_3$

Shuo Li,^{1,2,*} Zhanlong Wu,^{1,*} Yanhong Wang,^{3,*} Jun Luo,² Kefan Du,¹ Xiaoyu Xu,¹ Ze Hu,¹ Ying Chen,¹ Jie Yang,² Zhengxin Liu,^{1,4} Rong Yu,^{1,4} Yi Cui,^{1,4,†} Rui Zhou,^{2,‡} Hongcheng Lu,^{3,§} and Weiqiang Yu^{1,4,¶}

¹*School of Physics and Beijing Key Laboratory of Opto-electronic Functional Materials & Micro-nano Devices, Renmin University of China, Beijing 100872, China*

²*Institute of Physics, Chinese Academy of Sciences, and Beijing National Laboratory for Condensed Matter Physics, Beijing 100190, China*

³*School of Chemistry and Chemical Engineering, Huazhong University of Science and Technology, Wuhan, 430074, China*

⁴*Key Laboratory of Quantum State Construction and Manipulation (Ministry of Education), Renmin University of China, Beijing 100872, China*

We performed single-crystal magnetic susceptibility and ^1H NMR measurements on a quasi-1D, spin-1 antiferromagnet $\text{NiC}_2\text{O}_4 \cdot 2\text{NH}_3$, with temperature down to 100 mK and with field up to 26 T. With field applied along the chain direction (crystalline b direction), a spin gap is determined at low fields. Our susceptibility and spin-lattice relaxation measurements reveal a Haldane phase at low field, with an intrachain exchange coupling $J \approx 35$ K and an easy-plane single-ion anisotropy of 17 K. A field-induced antiferromagnetic (AFM) ordering emerges at fields of 2.1 T, which sets a three-dimensional (3D) quantum critical point (QCP). The high-temperature spin-lattice relaxation rates $1/T_1$ resolves an onset of Tomonaga-Luttinger liquid behavior at field above 3.5 T, which characterizes a hidden 1D QCP.

I. INTRODUCTION

After Haldane's conjecture in 1983¹, Heisenberg antiferromagnetic (HAFM) chains with integer spins have attracted a lot of interests. In contrast to half-integer spin chains with gapless, continuum excitations, the integer spin HAFM chains are equivalent to a valence-bond-solid (VBS) state without long-range magnetic ordering and depicted by a hidden string order, representing the breaking of non-local hidden symmetries²⁻⁴. A closely related 1D, spin-1 chain with AFM interaction was precisely solved by Affleck, Kennedy, Lieb, and Tasaki (AKLT)⁵, and Haldane phase can be adiabatically connected to the AKLT state⁵, which is a one-dimensional (1D) magnetic symmetry-protected-topological (SPT) phase containing a bulk triplet gap Δ and a gapless edge mode^{1,6}. With application of external field above a critical value, a gapless Tomonaga-Luttinger liquid (TLL) is induced⁷⁻⁹.

In bulk materials, single-ion anisotropy (D) and interchain couplings (J') are inevitable, which could suppress the AKLT state and lead to other phases^{10,11}. As presented by a phase diagram in the D - J' plane, the Haldane phase is confined in a limited parameter space, neighboring AFM and gapped large- D phases¹². Up to now, several nickelate magnets were reported as the Haldane systems, notably $\text{Ni}(\text{C}_2\text{H}_8\text{N}_2)_2\text{NO}_2\text{ClO}_4$ (NENP)¹³⁻²¹, $\text{Ni}(\text{C}_5\text{H}_{14}\text{N}_2)_2\text{N}_3(\text{PF}_6)$ (NDMAP)^{22,23}, Y_2BaNiO_5 ^{24,25}, and some others²⁶⁻³¹. In NENP, the spin gap^{13,14,17-20,32} and a field-induced staggered transverse magnetization³³ were reported. Experimental verifications of Haldane phase and its novel excitations are still demanding in the context of topological phases.

The Hamiltonian for the intrachain couplings of quasi-1D, AFM spin-1 materials is expressed as³⁴,

$$H = \sum_i J \vec{S}_i \cdot \vec{S}_{i+1} + D(S_i^z)^2 + E[(S_i^x)^2 - (S_i^y)^2], \quad (1)$$

where J (>0) represents exchange couplings, D and E rep-

resent single-ion anisotropy which are caused by spin-orbit coupling and crystal field. The Haldane phase exists in a range of D values between $-0.29J \leq D \leq 0.99J$ ^{35,36}. For $D > 0.99J$, the ground state is the large- D state which is gapped and topologically trivial³⁷.

For the isotropic limit ($D = E = 0$), the Haldane phase is characterized by triplet excitations with a minimum gap $\Delta = 0.41J$ at $q = \pi$ and a gap 2Δ at $q = 0$, above which two-particle continuum emerges^{38,39}. The addition of the D term splits the triplet excitations into anisotropic excitations, including a singlet with a gap Δ_z and a doublet with a gap Δ_{xy} ^{19,40}. For $0 \leq D \leq 0.25J$, these two gaps scale linearly with D by^{19,40}

$$\Delta_z = 0.41J + 1.41D, \Delta_{xy} = 0.41J - 0.57D. \quad (2)$$

Δ_{xy} will further split with the in-plane anisotropy term E .

Recently, a quasi-1D, spin-1 compound $\text{NiC}_2\text{O}_4 \cdot 2\text{NH}_3$ (NiCO) was reported⁴¹. In this paper, we report single-crystal ^1H NMR measurements down to 100 mK and with fields up to 26 T, and susceptibility measurements down to 2 K. With field applied along the crystalline b axis (chain direction), we found that the system follow the Haldane physics with an easy-plane single-ion anisotropy D and negligible in-plane anisotropy E .

The ground state is gapped with $\Delta_{xy} = 4.9$ K, which closes at a 3D critical field $H_c^{3D} \approx 2.1$ T. Beyond H_c^{3D} , a glassy behavior is observed and a field-induced magnetic ordering occurs at low temperatures with magnetic field above H_c^{AFM} (2.44 T). With field above 3.5 T, a power-law scaling between $1/T_1$ and temperature is found above T_N , which characterizes a TLL liquid behavior and a hidden 1D critical field H_c^{1D} (3.5 T). The model parameters of the system are then determined as $J \approx 35$ K, $D \approx 0.47(4)J$, $E \approx 0$ and $J' \approx 0.022J$.

The paper is organized as the following. Materials and experimental methods are presented in Sec. II. In Sec. III, magnetic susceptibility of $\text{NiC}_2\text{O}_4 \cdot 2\text{NH}_3$ measured with different field orientations are analyzed. In Sec. IV, NMR spectra at

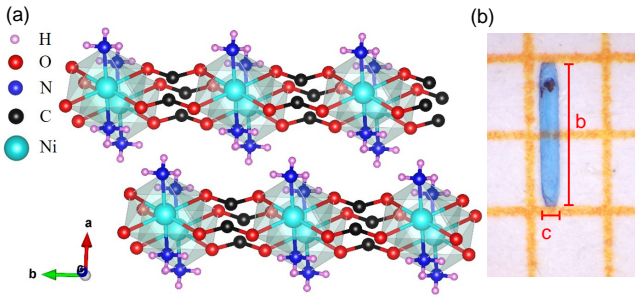


FIG. 1. **Lattice structure of NiCO.** (a) Lattice structure viewed along the c axis. NiO_4N_2 octahedra and shared $\text{C}_2\text{O}_4^{2-}$ unit are aligned in parallel along the b axis (the chain direction). NH_3 groups are located above and below the Ni^{2+} ions. (b) Picture of a NiCO single crystal with the b axis and c axis marked.

typical fields are shown, which resolves the distinction between the gapped Haldane phase and the ordered AFM phase. In Sec. V, $1/T_1$ are reported, where the Haldane gap Δ , the Néel temperature T_N , and Luttinger exponent η are determined. Finally, an (H, T) phase diagram is established and shown in Sec. VI.

II. MATERIALS AND METHODS

NiCO crystallizes in a centrosymmetric monoclinic structure in the space group $C2/m$ as shown in Fig. 1, with lattice parameters $a = 10.767 \text{ \AA}$, $b = 5.414 \text{ \AA}$ and $c = 5.005 \text{ \AA}$ ⁴¹. The material contains NiC_2O_4 octahedra, with Ni^{2+} strongly coupled along the crystalline b axis to form the spin-1 chain.

The NiCO single crystals were first synthesized using the hydrothermal method by Kenneth R. Poeppelmeier, who discovered that the material exhibits magnetic properties⁴¹. High-quality single crystals with typical dimensions of $0.5 \times 0.2 \times 0.1 \text{ mm}^3$ are chosen for the measurements. Bulk susceptibility were measured in a Quantum-Design magnetic property measurement system (MPMS) with field along different crystalline directions. NMR measurements were performed on ^1H nuclei (gyromagnetic ratio $\gamma = 42.5759 \text{ MHz/T}$). The sample was fixed in a silver coil with Cytop glue which is proton free, and cooled in a Variable Temperatures Insert (VTI) with temperature down to 1.8 K and in a dilution refrigerator with temperature down to 100 mK. NMR measurements above 16 T were performed Synergetic Extreme Condition User Facility (SECUF), with the 26T all-superconducting magnet.

^1H NMR spectra were collected by the spin-echo method, using $\pi/2 - \tau - \pi/3$ sequences, where $\pi/2$ and $\pi/3$ denote typical RF pulses for amino group, affected by proton rotation, with time durations of 5 \mu s and 3 \mu s , respectively. For broad spectra at high fields, the spectra were obtained by sweeping frequencies at fixed field. The NMR Knight shift was calculated by $K_n = (f/\gamma H - 1) \times 100\%$, where f is the average frequency of the whole spectrum.

The spin-lattice relaxation rates $1/T_1$ was measured by the spin inversion-recovery method. T_1 was obtained by fit-

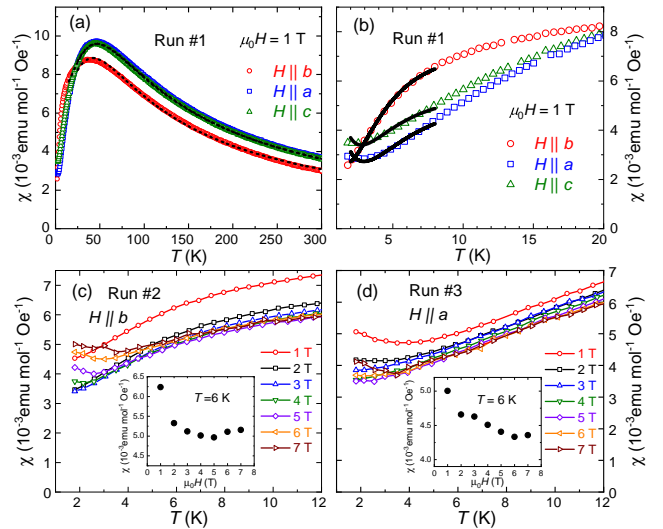


FIG. 2. **Magnetic susceptibility.** (a) χ as functions of temperatures at a field of 1 T, with the field applied along the crystalline a , b , and c axis, respectively. The dash lines represent high-temperature fits to Eq. 3, covering the temperatures from 300 K down to 30 K. (b) Enlarged view of the low-temperature data. The solid lines represent fits to Eq. 5. In (c) & (d), $\chi(T)$ is depicted as functions of temperatures for different fields applied along the a and b axis, respectively. Insets: χ as functions of fields at a constant temperature 1.8 K. Data for each panel were taken during separate experimental runs, as indicated in each panel.

ting the nuclear magnetization $m(t)$ to the recovery function $m(t) = m(\infty)[1 - ae^{-(t/T_1)^\beta}]$, where β is a stretching factor. β is found to be about 1 in the paramagnetic phase, which indicates high-quality of the sample.

III. BULK SUSCEPTIBILITY

The low-field magnetic susceptibility $\chi(T)$ were measured under a field of 1 T, applied along three crystalline axes respectively, with data shown in Fig. 2(a). Upon cooling, $\chi(T)$ first increases and exhibits a broad peak around 45 K with field along the a and the c axis, and at 37 K with field along the b axis, which is a typical behavior of 1D magnets⁴². At temperature above 50 K, χ shows nearly identical values with field along the a and c axis, but larger than that along the b axis, which suggests the presence of an easy-plane anisotropy D , whereas the in-plane anisotropy term E is likely very small.

We first attempt to fit the high-temperature χ to the form for an isotropic Haldane chain^{41,43},

$$\chi = \frac{N\mu_B^2 g^2}{k_B T} \frac{2 + 0.0194x + 0.777x^2}{3 + 4.346x + 3.232x^2 + 5.834x^3}, \quad (3)$$

where $x = J/k_B T$, and N , μ_B , g , and k_B are Avogadro constant, Bohr magneton, g -factor and Boltzmann constant, respectively. All fits, as demonstrated in Fig. 2(a), are succeeded with temperatures from 30 K to 300 K. The fitting parameters,

with three field orientations, are obtained as

$$\begin{aligned} J_a/k_B &= 35.6 \pm 0.1 \text{ K}, g_a = 2.30 \pm 0.01, \\ J_b/k_B &= 31.8 \pm 0.1 \text{ K}, g_b = 2.07 \pm 0.01, \\ J_c/k_B &= 35.0 \pm 0.1 \text{ K}, g_c = 2.27 \pm 0.01. \end{aligned} \quad (4)$$

The difference of J_a , J_b and J_c is within 15%, therefore a large D limit is ruled out³⁶. Considering that the susceptibility along the b axis is smaller than that along the a axis, it is suggested that $D > 0$. With this, we use $J = (J_a + J_c)/2 \approx 35.3 \text{ K}$ as the dominant term of the system.

Below 20 K, the sharp drop of χ upon cooling is a signature of gap opening. In fact, the data can be fit to combined contributions from both 1D gapped excitations²¹ and a Schottky-like term by

$$\chi \sim aT^{-0.5} \exp(-\Delta/T) + n \tanh\left(\frac{\mu_B B}{k_B T}\right), \quad (5)$$

where χ , Δ , B and n is magnetic susceptibility, energy gap, magnetic field and density of impurities respectively. The Schottky-like term catches the upturn observed at temperature below 2 K, with $H||a$ and $H||c$, as illustrated in Fig. 2(b). This upturn is likely due to the presence of magnetic impurities within the material. The gaps are obtained as $\Delta_a = 9.92 \text{ K}$, $\Delta_b = 7.10 \text{ K}$, and $\Delta_c = 8.41 \text{ K}$ at 1 T with three field orientations, by fits in a temperature range from 2 K to 8 K, as shown in Fig. 2(b). As χ is dominated by excitations at $q = 0$, the Haldane gap is estimated to be $\Delta_{xy} = \Delta_b/2 \approx 3.55 \text{ K}$ at 1 T, whereas the larger gap Δ_z may not be observable in χ at such low temperatures. Given that $\Delta_{xy} = 0.41J - 0.57D$ (see Eq. 1), D is estimated as $0.47 J$, which indicates that the system belongs to the Haldane class with an easy-plane anisotropy^{21,44-46}. The value of Δ_{xy} and D will be further confirmed by subsequent NMR measurements.

To elucidate the intrinsic behavior of the materials, χ are measured as functions of temperature, under various magnetic field strengths and orientations, as illustrated in Fig. 2(c)-(d). As the magnetic field increases, the upturn of magnetic susceptibility is diminished, resembling the behavior of free magnetic impurities. We then plotted χ as a function of magnetic field, at temperature about 6 K where the upturn is negligibly small, as shown in the inset of Fig. 2(c)-(d). A non-monotonic behavior is then seen with fields both along b and a axis respectively, which suggests a field induced critical behavior. With field along the b axis, a 1D quantum critical point is suggested at approximately 4 T, where $\chi(H)$ exhibits a dip feature. In fact, our spin-lattice relaxation rate $1/T_1$, as shown later, resolves a field-induced TLL behavior at fields above 3.5 T.

IV. NMR SPECTRA

In the following, the ^1H NMR spectra are presented, as shown in Fig. 3, which reveal a Haldane phase at low fields and a field-induced AFM ordering at high fields, as described below.

A. Paramagnetic and Haldane phase

The ^1H NMR spectra under a field of 2 T applied along the b axis, are shown with temperatures from 30 K down to 0.5 K, in Fig. 3(a). Three resonance peaks, marked by &1, &2 and &3, can be distinguished at high temperatures, which correspond to three hydrogen positions within the NH_3 group. The spectral width, as determined by the full-width at half-maximum (FWHM), measures approximately 51 kHz across the entire temperature range, although a smearing of three peaks is observed below 2 K. The entire spectrum shifts toward higher frequencies with decreasing temperature below approximately 30 K.

B. Knight shift

In fact, the Knight shift K_n , as depicted in Fig. 3(f), is calculated from the resonance frequency of the middle peak in the spectrum, which increases sharply as the temperature decreases.

As shown by the inset of Fig. 3(f), K_n are plotted against χ , with data measured at various temperatures and a magnetic field of 8 T. The data ranging from 40 K to 120 K conform to a linear fit, represented by the straight line. From which, the hyperfine coupling is determined to be $A_{\text{hf}} \approx -0.471 \text{ kOe}/\mu_B$.

With such a negative hyperfine coupling, the onset of a gapped phase is characterized by a sharp increase in the Knight shift. With decreasing temperature, K_n first decreases and then increases when cooled below 30 K, which is consistent with the change in the magnetic susceptibility, as depicted in Fig. 2(a). In particular, K_n at 2 T shows a very dramatic increase at temperatures below 20 K. At a field of 8 T, K_n approaches a finite value at the zero temperature limit, indicating the closure of the energy gap. This behavior is consistent with the presence of canted magnetization in the field-induced AFM phase.

C. High-field ordered AFM phase

To precisely determine the critical field that separates the Haldane phase from the ordered AFM phase, the spectra were measured at 100 mK with increasing fields, as illustrated in Fig. 3(b). The spectra are narrow at low fields from 1 T to 2.1 T, and a reduction in spectral intensity is observed at 2.1 T, which we identify as the critical magnetic field. A broad shouldered feature appears at a field of 2.2 T, with this shouldered feature serving as a signature of short-range AFM ordering. At 2.3 T, the spectral weight at the shoulders grows larger than the center peak. At 3 T, a broad spectrum is observed with several peaked features, indicating the presence of different hyperfine fields on different hydrogen sites due to magnetic ordering.

The magnetic transition at high fields with varying temperature can also be resolved. As shown in Fig. 3(c), spectra at a field of 2.8 T are measured over a temperature range from

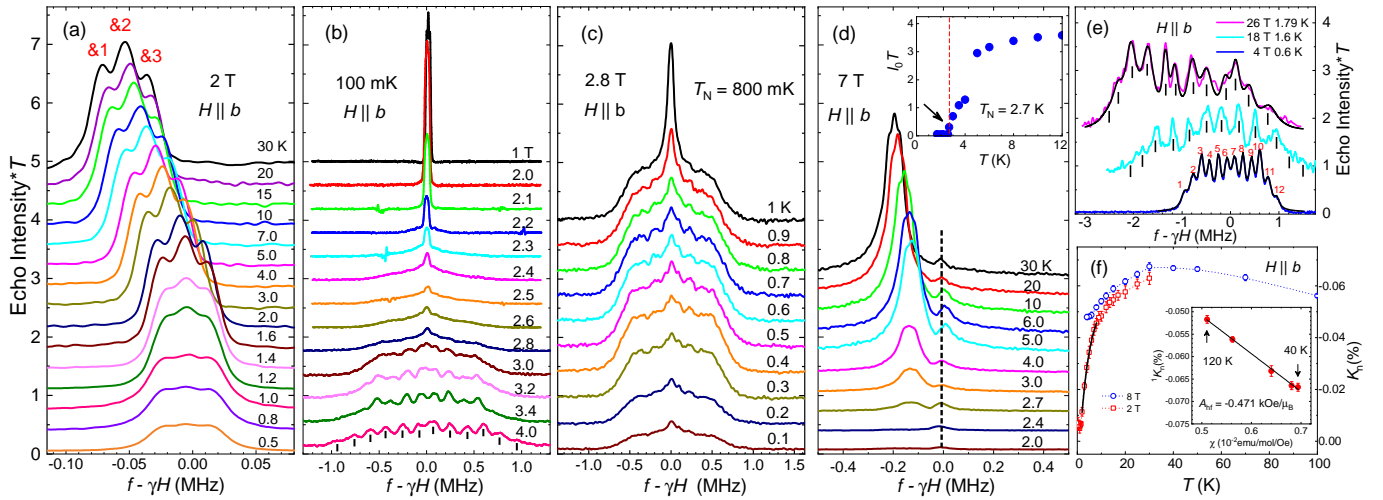


FIG. 3. ^1H NMR spectra with fields applied along the b axis. (a) Spectra measured at a field of 2 T, with three peaks labeled as &1, &2, and &3. (b) Ultra-low temperature spectra with fields ranging from 1 T to 4 T. The positions of NMR peaks at 4 T are indicated by vertical lines. (c) Spectra at 2.8 T, with T_N determined to be 800 mK from the disappearance of the sharp central peak. (d) Spectra measured at 7 T. The black dotted line points to a spurious ^1H peak. Inset: The integrated spectral weight as a function of temperature. The arrow marks T_N , which is set by a 90% intensity reduction in this study. (e) Spectra with fields of 4 T, 18 T and 26 T. Twelve NMR peaks are labeled by numbers (at 4 T) or the vertical lines (at 18 T and 26 T). The black solid lines, overlapping the 4 T and 26 T data, represent Lorentzian fits to the spectra, which include the twelve peaks. (f) K_n plotted as a function of temperature at typical fields of 2 T and 8 T, below and above the field-induced phase transition. Inset: K_n as a function of χ , measured at different temperatures and a constant field of 8 T, with the hyperfine coupling constant obtained by a linear fit to the data.

1 K down to 0.1 K. Upon cooling, the NMR spectrum is significantly broadened. At 1 K, a central peak with a FWHM of approximately 0.1 MHz, which contains overlapped ^1H contributions, is observed at the central position. However, broad shoulders are observed on both sides, indicating the development of short-range AFM ordering. When cooled below 0.8 K, the sharp peak become barely resolvable, and the FWHM of the whole spectrum reaches approximately 1 MHz, clearly indicating the onset of field-induced magnetic ordering. Here we define T_N (≈ 0.8 K), which marks the emergence of long-range ordering and is characterized by the strong suppression of the central paramagnetic peak. At a higher field of 7 T, the spectra measured at temperatures from 30 K to 2 K are displayed in Fig. 3(d). A single peak is observed down to 2 K, however, the spectral weight is clearly reduced upon cooling, indicating the emergence of magnetic ordering. For consistency, we define the Néel temperature T_N as the temperature at which 90% of the paramagnetic signal is lost, as illustrated in the inset of Fig. 3(d). The T_N , determined by this scheme, is consistent with the value determined from the peaked feature in the $1/T_1$, as demonstrated in the subsequent section.

We further performed NMR measurements in the high-field magnet at SECUF, with fields of 18 T and 26 T, as depicted in Fig. 3(e). Comparing the spectra in the ordered phase, the 12-peak feature is consistently observed at all three fields, as indicated by the short vertical lines.

Indeed, the observed line splitting in the high-field, ordered phase is consistent with field-induced AFM ordering. We assume the magnetic structure depicted in Fig. 4(a), where the AFM ordered moment are arranged in the crystalline ac plane,

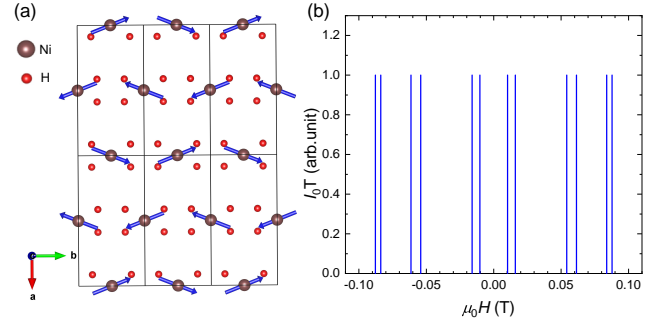


FIG. 4. **Spectral simulation of the field-induced AFM phase.** (a) Proposed magnetic structure of the field-induced AFM phase. (b) Simulated NMR spectra, assuming the magnetic structure shown in (a). In the simulation, the moment size along the respective a , b , and c directions is assumed with a ratio of 1:7:1 as an example.

perpendicular to the applied field (b axis), and a canted moment along the field direction. Using the dipolar-type hyperfine coupling, the NMR spectrum of this magnetic structure was simulated and presented in Fig. 4(b). The spectrum, which contains twelve peaks, is consistent with the observations shown in Fig. 3(e).

V. SPIN-LATTICE RELAXATION RATE

The NMR spin-lattice relaxation rate $1/T_1$, with $1/T_1 = \gamma^2 k_B T / \mu_B^2 \sum_q A_{\text{hf}}^2(q) \text{Im} \chi'(q, \omega) / \omega$, probes the low-energy fluctuation in the system, where $\chi'(q, \omega)$ is dynamic suscepti-

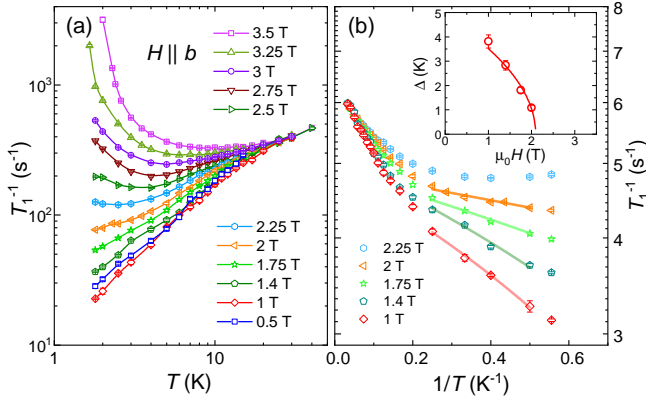


FIG. 5. $1/T_1$ at low fields. (a) $1/T_1$ as functions of temperatures measured with field from 0.5 T to 3.5 T. (b) Semilog plot of $1/T_1$ as functions of $1/T$ with field up to 2.25 T. The straight lines represent gap function fits to the data at low temperatures (see text). Inset: The obtained gap value Δ as a function of field. The solid line is a function fit to $\Delta(H) \sim (H_c - H)^{1/2}$ with field $H_c = 2.1$ T.

bility, $A_{\text{hf}}(q)$ is hyperfine coupling constant, and ω is Larmor frequency. In the following section, we present $1/T_1$ measured on ^1H at various magnetic fields.

A. Low-field Haldane phase

The $1/T_1$ measured at low fields along the b axis, is presented in Fig. 5 over a temperature range from 50 K to 1.8 K. Upon cooling below 30 K, $1/T_1$ initially decreases rapidly, consistent with the 1D behavior observed at temperatures below J^{42} . In the low-field range from 0.5 T to 2 T, a monotonic decrease of $1/T_1$ with temperature indicates that the system remains in the gapped Haldane phase. Above fields of 2.25 T, an upturn is evident upon further cooling, suggesting that the Haldane phase is suppressed. The system then enters the field-induced TLL phase (above T_N) and the ordered AFM phase (below T_N) respectively. This phase will be discussed in more detail later.

The spin gap in the Haldane phase can be deduced from the low-temperature behavior of $1/T_1$, which follows a gap function given by $1/T_1 \propto e^{-\Delta/T}$. The fitting is illustrated by a semilog plot of $1/T_1$ as a function of $1/T$, where the low temperature data follows a straight line for each field below 2 T. Indeed, such a fitting is only observed at temperatures significantly lower than Δ , as suggested by recent theoretical work⁴⁷. The gap Δ at each field is then determined from the slope of the line, with Δ depicted as a function of field in the inset of Fig. 5(b). Indeed, $\Delta(H)$ follows a critical behavior described by $\Delta(H) \sim (H_c - H)^{1/2}$ with $H_c = 2.1$ T, as seen in the function fit of the figure. Such a strong suppression of the gap with increasing field deviates from a linear behavior, which suggests that the system is influenced by the interchain coupling, particularly when it is close to the field-induced magnetic ordering.

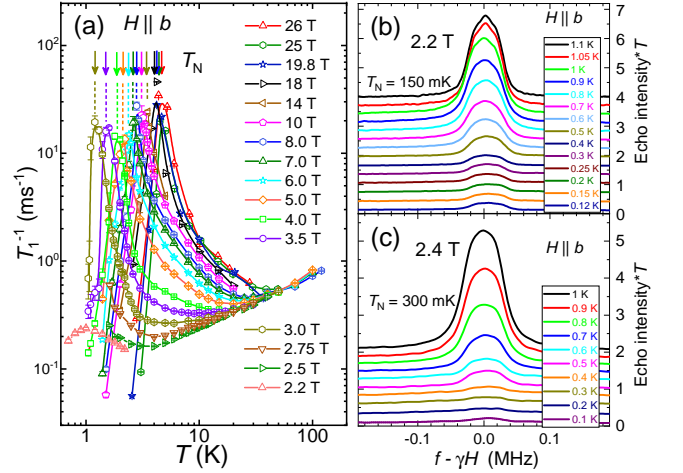


FIG. 6. $1/T_1$ at high fields. (a) $1/T_1$ as functions of temperatures. The arrows indicate the peak feature in $1/T_1$, which is used to determine the T_N as labeled. (b)-(c) Spectra at different temperatures, under field of 2.2 T and 2.4 T, respectively. The respective T_N at each field is defined as a temperature with 90% loss of paramagnetic spectral weight.

B. Field-induced AFM ordering

The $1/T_1$ with fields ranging from 2.2 T to 26 T are presented in Fig. 6(a) as functions of temperature. The measurement was also taken on the middle peak of the spectra for each field. For all these field, a peaked behavior at low temperatures is observed in $1/T_1$, which indicates the onset of field-induced magnetic ordering. The peak position corresponds to T_N , which is produced by strong low-energy spin fluctuations.

At fields of 3 T and above, a pronounced peak is observed in $1/T_1$, which clearly characterizes the phase transition temperature T_N , followed by the AFM ordering upon further cooling. The sharp drop in $1/T_1$ below T_N indicates spin-wave excitations. With increasing field up to 26 T, T_N shifts to higher temperatures.

With field ranging from 2.2 T to 3 T, the peak feature in $1/T_1$ is not prominent. Then we performed a spectral weight analysis to determine T_N , as illustrated in Fig. 6(b) and (c). At a field of 2.2 T, when the sample is cooled from 1.0 K to 0.1 K, a loss of spectral weight is observed at the center peak, which suggests the onset of very slow spin fluctuations or a glassy behavior that suppresses the spectra before reaching the ordered phase. For consistency, we define T_N as the temperature at which a 90% loss of spectral weight is observed at the center peak, which corresponds to 0.15 K at this field. A similar loss of spectral weight is observed at other fields above the critical field of 2.1 T, and the corresponding T_N at 2.4 T is determined to be 0.3 K as shown in Fig. 6(c).

Subsequently, all the T_N are obtained by these two methods and are depicted in the phase diagram shown in Fig. 8(a). The 3D quantum critical point between Haldane phase and AFM ordering is determined to be $H_c^{3D} \approx 2.1$ T, which is lower than the 1D QCP (3.5 T). This 1D QCP is determined by the

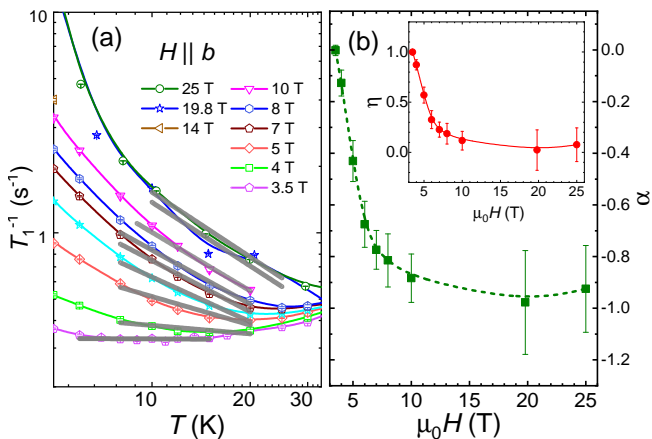


FIG. 7. **Spin-lattice relaxation rates in high-field PM phase.** (a) An enlarge view of $1/T_1$ data between 4 K and 30 K. The straight gray lines represent power-law fits (see text) to the data far above T_N (see text). (b) Power law exponent α at different field obtained from the fits. Inset: The Luttinger exponent η ($= \alpha - 1$) as a function of field.

high-temperature behavior of $1/T_1$ and will be further analyzed later.

For quasi-1D $S = 1$ HAFM chain, T_N can be approximated by the formula $T_N \approx (8J|J'|)^{1/221}$. Applying this to NiCO, with $T_N = 4$ K at a field far above the critical field, the interchain coupling J' is estimated to be approximately 0.77 K. T_N increase monotonically with the field up to 26 T, indicating that the fully polarized phase is at a very high field that was not achieved in the current study. Using the above parameters, the QCP for the fully polarized phase is estimated to be $H_{c2} \approx 99.5$ T, deduced by $H_{c2} \approx 4J/g\mu_B$ ^{48,49}.

C. High-field Tomonaga-Luttinger liquid behavior

With fields ranging from 2.2 T to 3 T, $1/T_1$ exhibits a dip feature at temperature between 3 K and 10 K (Fig. 6(a)), which should indicate a dimensional crossover behavior. At high temperatures, the phase is characterized by the 1D, Haldane gapped behavior, while at low temperatures, the phase is affected by the 3D coupling which enhances spin fluctuations and leads to AFM ordering. Therefore a 1D QCP is hidden within the 3D ordering regime. In the following analysis, we will determine the 1D QCP using the high-temperature $1/T_1$ data, where a TLL phase is established.

In a Haldane chain system without in-plane anisotropy, the suppression of the Haldane gap by an external field should lead to a TLL state characterized by gapless excitations^{50,51}. In the TLL state, the correlation function exhibit power-law decays with both a transverse and a longitudinal mode, which is written as

$$\begin{aligned} \langle S_0^x S_r^x \rangle &\sim (-1)^r r^{-\eta_x}, \\ \langle S_0^z S_r^z \rangle &> -M^2 \sim \cos(2K_F r) r^{-\eta_z}. \end{aligned} \quad (6)$$

In the TLL state, there is a relation $\eta_z \eta_x = 1$, where η are

the Luttinger exponent⁵². Consequently, the spin-lattice relaxation rates are expected to follow a power-law temperature dependence, given by $1/T_1 \approx cT^\alpha$, where $\alpha = \eta - 1$ and $\alpha = 1/\eta - 1$ for transverse and longitudinal AFM fluctuations, respectively⁵³.

This is indeed can be observed through the behavior of $1/T_1$ at temperatures far above T_N , where the interchain coupling J' is not effective. In the temperature regime just below 30 K, $1/T_1$ exhibits a power-law temperature dependence, $1/T_1 \sim T^\alpha$, as evidenced by the straight fit lines for fields ranging from 3.5 T and above. The power-law exponents α are plotted as a function of field, starting from zero at 3.5 T and monotonically decreasing to -0.9 at 25 T, clearly demonstrating the presence of gapless excitations.

For the Haldane model with $D > 0$, when a field is applied along the hard-axis (b direction in NiCO), transverse correlations should dominate the low-energy spin fluctuations. We then adopted $\eta = \alpha + 1$ and calculated η as a function of field, as shown in the inset of Fig. 6(b). The value of η starts at 1 at 3.5 T, decreases monotonically as field increases, and approaches zero at 25 T.

The emergence of power-law scaling in $1/T_1$ supports the existence of a hidden 1D QCP at 3.5 T, marking a transition from a gapped Haldane phase to a gapless TLL phase. The presence of gapless TLL behavior suggests that the in-plane anisotropy E should be negligible. Consequently, the high-field magnetic ordering could be effectively described by a magnetic Bose-Einstein condensation (BEC) model.

VI. PHASE DIAGRAM AND DISCUSSIONS

Our results are summarized in the H - T phase diagram, as illustrated in Fig. 8. T_N grows monotonically with field, but only reaches 4.5 K at 26 T, which suggests a large intrachain coupling and a small interchain coupling. Even with such a small interchain coupling, our data resolves two QCPs nearby, that is, a 3D QCP H_c^{3D} at about 2.1 T and a hidden 1D QCP H_c^{1D} at about 3.5 T, determined by the closure of the Haldane gap at low temperatures and the onset of the TLL behavior at high temperatures, respectively.

With field far less than H_c^{3D} , the interlayer coupling is negligible in gapped Haldane phase. By extrapolation, $\Delta_{xy} = \Delta(H = 0) \approx 4.9$ K $\approx 0.14J$ is obtained. Then with Eq. 2, $D \approx 0.47J$ is again estimated, consistent with that obtained by the susceptibility data. With above data, the determined parameters in the current study are listed in Table I. From which, we can conclude that the NiCO exhibits an easy-plane anisotropy, with single-ion anisotropy parameter $D > 0$ and $E \approx 0$.

In principle, the T_N of the AFM order should follow a power-law scaling $T_N \sim (H_c^{\text{AFM}} - H)^\beta$. As shown by the fits (black solid lines) in the inset of Fig. 8, we determine with $H_c^{\text{AFM}} \approx 2.439$ T and $\beta = 0.40682$, which is consistent with a 3D QCP of BEC⁵⁴. However, we observe a deviation from the fitting at fields below 2.44 T, as depicted in the enlarged view of the phase diagram in the inset of Fig. 8, which may be affected by disorder which helps to suppress the Haldane gap

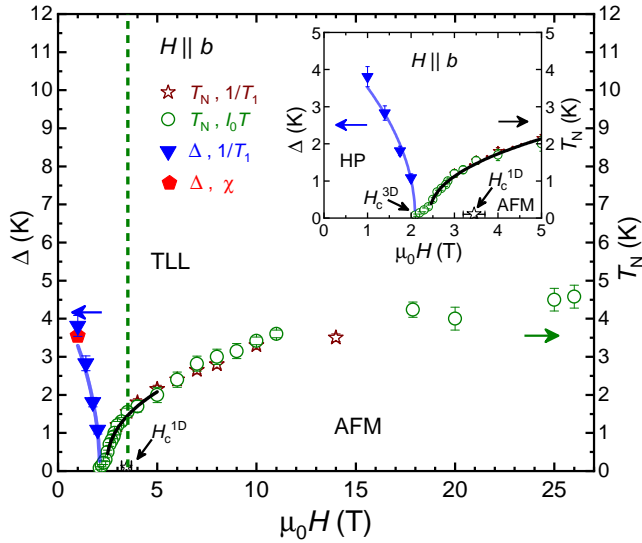


FIG. 8. **Phase Diagram.** The Haldane gap Δ and the phase boundaries between the Haldane phase and the ordered AFM phase determined by various probes. Δ intercepts the x -axis at H_c^{3D} , and the vertical line, representing the left boundary of the TLL phase, intercepts the x axis at the H_c^{1D} . The solid blue and black lines represent fits of Δ and T_N to power-law functions (see text). Inset: Enlarged view of Δ and T_N at low fields.

TABLE I. The parameters obtained by different measurements in this work.

	J	Δ_{xy}	Δ_{xy}	D
	35 K	3.55 K	4.9 K	16.58 K
Methods[field]	χ [1T]	χ [1T]	$1/T_1$ [0T]	$1/T_1$

at low fields.

VII. SUMMARY

To summarize, we conducted susceptibility and NMR studies on the spin-1 chain compound $\text{NiC}_2\text{O}_4 \cdot 2\text{NH}_3$. Our data reveal a gapped Haldane phase at low fields and a field-induced magnetic ordering with field above a 3D quantum critical point H_c^{3D} of approximately 2.1 T. Additionally, Tomonaga-Luttinger liquid(TLL) behavior is observed in the field range above a 1D quantum critical point H_c^{1D} (≈ 3.5 T), at temperatures above T_N . With analysis data of the susceptibility and NMR data, we estimated the dominant intrachain exchange coupling to be approximately $J \approx 35$ K, with an easy-plane single-ion anisotropy of $D \approx 0.47 J$ and a negligible in-plane anisotropy E .

VIII. ACKNOWLEDGEMENTS

The authors thank Professors Fenghua Ding, Kent Griffith and Kenneth Poepplmeier for communicating their initial synthesis, structural and magnetic results. This work is supported by the National Key R&D Program of China (Grant No. 2023YFA1406500, No. 2022YFA1402700, No. 2023YFA1406100 and No. 2022YFA1403402), the National Natural Science Foundation of China (Grant No. 12134020, No. 12374156, No. 12104503, No. 12374142 and No. 12304170), and the Strategic Priority Research Program(B) of the Chinese Academy of Sciences(Grant No.XDB33010100). A portion of this work was carried out at the Synergetic Extreme Condition User Facility (SECUF).

* These authors contributed equally to this study.

† cuiyi@ruc.edu.cn

‡ rzhou@iphy.ac.cn

§ hcl@hust.edu.cn

¶ wqyu_phy@ruc.edu.cn

¹ F. D. M. Haldane, “Nonlinear Field Theory of Large-Spin Heisenberg Antiferromagnets: Semiclassically Quantized Solitons of the One-Dimensional Easy-Axis Néel State,” *Phys. Rev. Lett.* **50**, 1153 (1983).

² M. den Nijs and K. Rommelse, “Preroughening transitions in crystal surfaces and valence-bond phases in quantum spin chains,” *Phys. Rev. B* **40**, 4709 (1989).

³ T. Kennedy and H. Tasaki, “Hidden symmetry breaking and the Haldane phase in S=1 quantum spin chains,” *Commun. Math. Phys.* **147**, 431 (1992).

⁴ S. Yamamoto and S. Miyashita, “Thermodynamic properties of S=1 antiferromagnetic Heisenberg chains as Haldane systems,” *Phys. Rev. B* **48**, 9528 (1993).

⁵ I. Affleck, T. Kennedy, E. H. Lieb, and H. Tasaki, “Rigorous results on valence-bond ground states in antiferromagnets,” *Phys. Rev. Lett.* **59**, 799 (1987).

⁶ T.-K. Ng, “Edge states in antiferromagnetic quantum spin chains,” *Phys. Rev. B* **50**, 555 (1994).

⁷ H. J. Schulz, “Critical behavior of commensurate-incommensurate phase transitions in two dimensions,” *Phys. Rev. B* **22**, 5274 (1980).

⁸ T. Giamarchi, *Quantum Physics in One Dimension* (Oxford University Press, 2003).

⁹ M. Sato, “Bosonic representation of spin operators in the field-induced critical phase of spin-1 Haldane chains,” *J. Stat. Mech.*

- Theory Exp* **2006**, P09001 (2006).
- ¹⁰ H. J. Schulz, "Phase diagrams and correlation exponents for quantum spin chains of arbitrary spin quantum number," *Phys. Rev. B* **34**, 6372 (1986).
 - ¹¹ A. K. Bera, B. Lake, A. T. M. N. Islam, B. Klemke, E. Faulhaber, and J. M. Law, "Field-induced magnetic ordering and single-ion anisotropy in the quasi-one-dimensional Haldane chain compound $\text{SrNi}_2\text{V}_2\text{O}_8$: A single-crystal investigation," *Phys. Rev. B* **87**, 224423 (2013).
 - ¹² E. S. Kozlyakova, A. V. Moskin, P. S. Berdonosov, V. V. Gapontsev, S. V. Streltsov, M. Uhlarz, S. Spachmann, A. ElGhandour, R. Klingeler, and A. N. Vasiliev, "Quasi-1D XY antiferromagnet $\text{Sr}_2\text{Ni}(\text{SeO}_3)_2\text{Cl}_2$ at Sakai-Takahashi phase diagram," *Sci. Rep* **11**, 15002 (2021).
 - ¹³ W. J. L. Buyers, R. M. Morra, R. L. Armstrong, M. J. Hogan, P. Gerlach, and K. Hirakawa, "Experimental evidence for the Haldane gap in a spin-1 nearly isotropic, antiferromagnetic chain," *Phys. Rev. Lett.* **56**, 371 (1986).
 - ¹⁴ J. P. Renard, M. Verdaguer, L. P. Regnault, W. A. C. Erkelens, J. Rossat-Mignod, and W. G. Stirling, "Presumption for a Quantum Energy Gap in the Quasi-One-Dimensional $S=1$ Heisenberg Antiferromagnet $\text{Ni}(\text{C}_2\text{H}_8\text{N}_2)_2\text{NO}_2(\text{ClO}_4)$," *EPL* **3**, 945 (1987).
 - ¹⁵ J. P. Renard, M. Verdaguer, L. P. Regnault, W. A. C. Erkelens, J. Rossat-Mignod, J. Ribas, W. G. Stirling, and C. Vettier, "Quantum energy gap in two quasi-one-dimensional $S=1$ Heisenberg antiferromagnets (invited)," *J. Appl. Phys.* **63**, 3538 (1988).
 - ¹⁶ Y. Ajiro, T. Goto, H. Kikuchi, T. Sakakibara, and T. Inami, "High-field magnetization of a quasi-one-dimensional $S=1$ antiferromagnet $\text{Ni}(\text{C}_2\text{H}_8\text{N}_2)_2\text{NO}_2(\text{ClO}_4)$: Observation of the Haldane gap," *Phys. Rev. Lett.* **63**, 1424 (1989).
 - ¹⁷ T. Goto, N. Fujiwara, T. Kohmoto, and S. Maegawa, "Proton Spin-Lattice Relaxation in the Quasi-One-Dimensional $S=1$ Heisenberg Antiferromagnet $\text{Ni}(\text{C}_2\text{H}_8\text{N}_2)_2\text{NO}_2(\text{ClO}_4)$," *J. Phys. Soc. Jpn.* **59**, 1135 (1990).
 - ¹⁸ N. Fujiwara, T. Goto, S. Maegawa, and T. Kohmoto, "Experimental evidence for the lowest excitation mode in the $s=1$ Haldane-gap system: High-field proton magnetic relaxation in $\text{Ni}(\text{C}_2\text{H}_8\text{N}_2)_2\text{NO}_2(\text{ClO}_4)$," *Phys. Rev. B* **45**, 7837 (1992).
 - ¹⁹ L. C. Brunel, T. Brill, I. Zaliznyak, J. P. Boucher, and J. P. Renard, "Magnon spin resonance in the Haldane spin chains of $\text{Ni}(\text{C}_2\text{H}_8\text{N}_2)_2\text{NO}_2(\text{ClO}_4)$," *Phys. Rev. Lett.* **69**, 1699 (1992).
 - ²⁰ L.P. Regnault and J.P. Renard, "Spin dynamics under high magnetic field in the haldane-gap system nennp," *Physica B: Condensed Matter* **234**, 541 (1997), proceedings of the First European Conference on Neutron Scattering.
 - ²¹ J. P. Renard, L. P. Regnault, and M. Verdaguer, "Haldane Quantum Spin Chains," *Magnetism: Molecules to Materials*, , 49–93 (2004).
 - ²² Z. Honda, K. Katsumata, H. Aruga Katori, K. Yamada, T. Ohishi, T. Manabe, and M. Yamashita, "Inducing a magnetic ordering in the Haldane material $\text{Ni}(\text{C}_5\text{H}_{14}\text{N}_2)_2\text{N}_3(\text{ClO}_4)$ by magnetic field," *J. Phys. Condens. Matter* **9**, L83 (1997).
 - ²³ Z. Honda, H. Asakawa, and K. Katsumata, "Magnetic Field versus Temperature Phase Diagram of a Quasi-One-Dimensional $S=1$ Heisenberg Antiferromagnet," *Phys. Rev. Lett.* **81**, 2566 (1998).
 - ²⁴ T. Shimizu, D. E. MacLaughlin, P. C. Hammel, J. D. Thompson, and S. W. Cheong, "Spin susceptibility and low-lying excitations in the Haldane-gap compound Y_2BaNiO_5 ," *Phys. Rev. B* **52**, R9835 (1995).
 - ²⁵ G. Y. Xu, J. F. DiTusa, T. Ito, K. Oka, H. Takagi, C. Broholm, and G. Aeppli, " Y_2BaNiO_5 : A nearly ideal realization of the $S = 1$ Heisenberg chain with antiferromagnetic interactions," *Phys. Rev. B* **54**, R6827 (1996).
 - ²⁶ J. P. Renard, V. Gadet, L. P. Regnault, and M. Verdaguer, "Experiments on Haldane gap in quasi-one-dimensional antiferromagnets," *J. Magn. Magn. Mater.* **90**, 213 (1990).
 - ²⁷ V. Gadet, M. Verdaguer, V. Briois, A. Gleizes, J. P. Renard, P. Beauvillain, C. Chappert, T. Goto, K. Le Dang, and P. Veillet, "Structural and magnetic properties of $(\text{CH}_3)_4\text{NNi}(\text{NO}_2)_3$: A Haldane-gap system," *Phys. Rev. B* **44**, 705 (1991).
 - ²⁸ T. Takeuchi, T. Yosida, K. Inoue, M. Yamashita, T. Kumada, K. Kindo, S. Merah, M. Verdaguer, and J.P. Renard, "Magnetic properties of new Haldane gap materials," *J. Magn. Magn. Mater.* **140**, 1633 (1995), international Conference on Magnetism.
 - ²⁹ Z. Honda, K. Katsumata, Y. Nishiyama, and I. Harada, "Field-induced long-range ordering in an $S = 1$ quasi-one-dimensional Heisenberg antiferromagnet," *Phys. Rev. B* **63**, 064420 (2001).
 - ³⁰ H. Tsujii, Z. Honda, B. Andracka, K. Katsumata, and Y. Takano, "High-field phase diagram of the Haldane-gap antiferromagnet $\text{Ni}(\text{C}_5\text{H}_{14}\text{N}_2)_2\text{N}_3(\text{PF}_6)$," *Phys. Rev. B* **71**, 014426 (2005).
 - ³¹ P. Tin, M. J. Jenkins, J. Xing, N. Caci, Z. Gai, R. Y. Jin, S. Wessel, J. Krzystek, C. Li, L. L. Daemen, Y. Q. Cheng, and Z. L. Xue, "Haldane topological spin-1 chains in a planar metal-organic framework," *Nat. Commun.* **14**, 5454 (2023).
 - ³² W. Lu, J. Tuchendler, M. von Ortenberg, and J. P. Renard, "Direct observation of the Haldane gap in NENP by far-infrared spectroscopy in high magnetic fields," *Phys. Rev. Lett.* **67**, 3716 (1991).
 - ³³ M. Chiba, Y. Ajiro, H. Kikuchi, T. Kubo, and T. Morimoto, "Transverse staggered moment in the Haldane-gap antiferromagnet $\text{Ni}(\text{C}_2\text{H}_8\text{N}_2)_2\text{NO}_2(\text{ClO}_4)$ observed by proton nuclear magnetic resonance," *Phys. Rev. B* **44**, 2838 (1991).
 - ³⁴ Y. C. Tzeng, H. Onishi, T. Okubo, and Y. J. Kao, "Quantum phase transitions driven by rhombic-type single-ion anisotropy in the $S = 1$ Haldane chain," *Phys. Rev. B* **96**, 060404 (2017).
 - ³⁵ T. Sakai and M. Takahashi, " $S=1$ antiferromagnetic Heisenberg chain with an axial-symmetry-breaking anisotropy," *Phys. Rev. B* **44**, 10385 (1991).
 - ³⁶ O. Golinelli, Th. Jolicoeur, and R. Lacaze, "Dispersion of magnetic excitations in a spin-1 chain with easy-plane anisotropy," *Phys. Rev. B* **46**, 10854 (1992).
 - ³⁷ S. V. Streltsov O. V. Maximova and A. N. Vasiliev, "Long range ordered, dimerized, large-D and Haldane phases in spin 1 chain compounds," *Crit. Rev. Solid State Mater. Sci.* **46**, 371 (2021).
 - ³⁸ G. Gómez-Santos, "Variational approach to the XXZ spin-1 linear chain: Elementary excitations and Haldane conjecture," *Phys. Rev. Lett.* **63**, 790 (1989).
 - ³⁹ S. R. White and D. A. Huse, "Numerical renormalization-group study of low-lying eigenstates of the antiferromagnetic $S=1$ Heisenberg chain," *Phys. Rev. B* **48**, 3844 (1993).
 - ⁴⁰ O. Golinelli, Th. Jolicoeur, and R. Lacaze, "Haldane gaps in a spin-1 Heisenberg chain with easy-plane single-ion anisotropy," *Phys. Rev. B* **45**, 9798 (1992).
 - ⁴¹ F. H. Ding, K. J. Griffith, C. Zhang, J. Zhan, H. C. Lu, and K. R. Poeppelmeier, "Synthesis, crystal structure, and magnetic properties of a one-dimensional chain antiferromagnet $\text{NiC}_2\text{O}_4 \cdot 2\text{NH}_3$," *J. Solid State Chem.* **314**, 123360 (2022).
 - ⁴² J. C. Bonner and M. E. Fisher, "Linear Magnetic Chains with Anisotropic Coupling," *Phys. Rev.* **135**, A640 (1964).
 - ⁴³ A. Meyer, A. Gleizes, J. J. Girerd, M. Verdaguer, and O. Kahn, "Crystal structures, magnetic anisotropy properties and orbital interactions in catena- $(\mu$ -nitrito)-bis(ethylenediamine)nickel(II) perchlorate and triiodide," *Inorg. Chem.* **21**, 1729 (1982).
 - ⁴⁴ I. Affleck, "Theory of electron spin resonance in Haldane-gap antiferromagnets," *Phys. Rev. B* **46**, 9002 (1992).
 - ⁴⁵ K. Wierschem and P. Sengupta, "Quenching the Haldane Gap in Spin-1 Heisenberg Antiferromagnets," *Phys. Rev. Lett.* **112**,

- 247203 (2014).
- ⁴⁶ W. Keola and S. Pinaki, “Characterizing the Haldane phase in quasi-one-dimensional spin-1 Heisenberg antiferromagnets,” *Mod. Phys. Lett. B* **28**, 1430017 (2014).
- ⁴⁷ S. Capponi, M. Dupont, A. W. Sandvik, and P. Sengupta, “NMR relaxation in the spin-1 Heisenberg chain,” *Phys. Rev. B* **100**, 094411 (2019).
- ⁴⁸ J. B. Parkinson and J. C. Bonner, “Spin chains in a field: Crossover from quantum to classical behavior,” *Phys. Rev. B* **32**, 4703 (1985).
- ⁴⁹ T. Sakai and M. Takahashi, “S=1 antiferromagnetic Heisenberg chain in a magnetic field,” *Phys. Rev. B* **43**, 13383 (1991).
- ⁵⁰ K. Okunishi and T. Suzuki, “Field-induced incommensurate order for the quasi-one-dimensional XXZ model in a magnetic field,” *Phys. Rev. B* **76**, 224411 (2007).
- ⁵¹ M. Klanjšek, H. Mayaffre, C. Berthier, M. Horvatić, B. Chiari, O. Piovesana, P. Bouillot, C. Kollath, E. Orignac, R. Citro, and T. Giamarchi, “Controlling Luttinger Liquid Physics in Spin Ladders under a Magnetic Field,” *Phys. Rev. Lett.* **101**, 137207 (2008).
- ⁵² N. Maeshima, K. Okunishi, K. Okamoto, and T. Sakai, “Frustration-Induced η Inversion in the $S = 1/2$ Bond-Alternating Spin Chain,” *Phys. Rev. Lett.* **93**, 127203 (2004).
- ⁵³ M. Klanjšek, M. Horvatić, S. Krämer, S. Mukhopadhyay, H. Mayaffre, C. Berthier, E. Canévet, B. Grenier, P. Lejay, and E. Orignac, “Giant magnetic field dependence of the coupling between spin chains in BaCo₂V₂O₈,” *Phys. Rev. B* **92**, 060408 (2015).
- ⁵⁴ C. Yasuda, S. Todo, K. Hukushima, F. Alet, M. Keller, M. Troyer, and H. Takayama, “Néel Temperature of Quasi-Low-Dimensional Heisenberg Antiferromagnets,” *Phys. Rev. Lett.* **94**, 217201 (2005).